CHEMISTRY OF MATERIALS

ARTICLE

pubs.acs.org/cm

Adsorption and Activation of CO_2 by Amine-Modified Nanoporous Materials Studied by Solid-State NMR and $^{13}CO_2$ Adsorption

Moisés L. Pinto,*[,†,‡] Luís Mafra,*[,‡] José M. Guil,[§] João Pires,[†] and João Rocha[‡]

[†]Department of Chemistry and Biochemistry and CQB, Faculty of Sciences, University of Lisbon, Ed. C8, Campo Grande, 1749-016 Lisboa, Portugal

[‡]Department of Chemistry, CICECO, University of Aveiro, 3810-193 Aveiro, Portugal

[§]Instituto de Química Física 'Rocasolano', CSIC, Serrano 119, E-28006 Madrid, Spain

Supporting Information

ABSTRACT: The interaction of gaseous CO_2 with the surface of amine-modified nanoporous clays has been studied. CO_2 adsorption and adsorption microcalorimetry revealed high adsorption capacity and strong interaction with the surface at low pressures, due to the presence of amine groups. Considerable surface heterogeneity and high initial adsorption heat (125 kJ mol^{-1}) have been observed, although the adsorption was reversible with hysteresis at low pressures and very slow desorption kinetics. Interaction between $^{13}CO_2$ and the surface of the nanoporous clay materials has been investigated by ^{13}C and ^{15}N magic-angle spinning (MAS) NMR. ^{13}C NMR resonances at ca. 164 and 160 ppm have been assigned to, respectively, carbamate and carbamic acid, and the stability of these species have been studied. Peak areas and the amount of $^{13}CO_2$ adsorbed allowed the determination of the concentration of carbamate and carbamic acid. To the best of our knowledge, this is the first time that solid-state NMR is used to clearly establish the formation of amine-CO_2 bonding at the surface of amine-modified nanoporous materials and to identify the nature of the species formed. The results presented here shed light on the mechanism of CO_2 activation, since the CO_2 adsorption on the surface of such materials is the activation step that allows further reactions to occur. The instability of the carbamate and carbamic acid species formed on the surface is important in explaining the reactivity of these intermediates and supports the possible application of these materials in CO_2 activation.

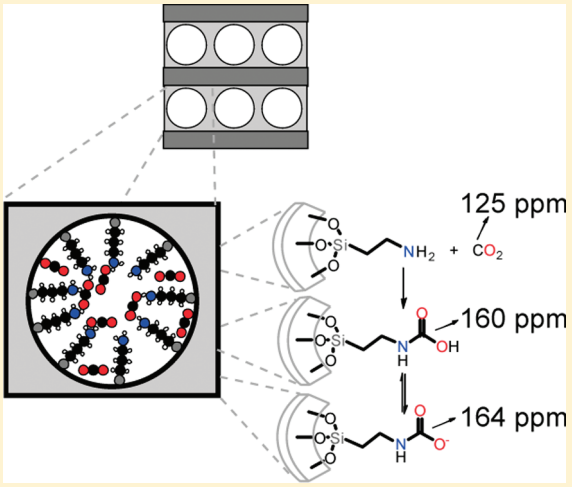

KEYWORDS: $^{13}CO_2$ adsorption, mesoporous materials, porous clays heterostructures, APTES, amine-functionalized materials

INTRODUCTION

The global awareness of the human impact on the Earth biosphere has increased considerably in recent years, especially concerning the problem of climate change. The majority of climate researchers agree that this phenomenon is associated with the high concentration of greenhouse gases in the atmosphere, particularly CO_2, which increased considerably during the second half of the last century.[1] An acceptable level for greenhouse gases in the atmosphere is still open to debate, but even modest stabilization scenarios will eventually require a reduction in worldwide greenhouse gas emissions to 50−90% of the current levels.

In recent years, carbon sequestration has been proposed to reduce atmospheric CO_2, especially from stationary sources.[2] Briefly, the basic idea is to separate the CO_2 from flue gas streams and to trap it in oceans, terrestrial ecosystems, and geological formations including depleted gas, oil, and coal formations. The costs of separation and capture are estimated to add to about three-fourths of the total costs of ocean or geologic sequestration and are thus the most important step in the economics of the process.[2] Beside sequestration, much research is directed to the application of CO_2 as a raw material in several production processes,[1,3,4] which also require CO_2 with a high degree of purity and, thus, a previous separation of the flue gases must be undertaken.

The application of amine-modified nanoporous materials in the separation of CO_2 from flue gas streams has been proposed.[5] These materials have some important advantages over the standard industrial amine solution process, which is known to pose corrosion and pollution problems and is not energetically efficient. Two different pathways have been explored in the search for alternatives to the standard amine solution process: the "molecular basket" approach, in which mesoporous materials are impregnated with amine-rich polymers,[6−13] and the "amine-grafting" approach, in

Received: June 1, 2010
Revised: December 14, 2010
Published: February 10, 2011

dx.doi.org/10.1021/cm1029563 | *Chem. Mater.* 2011, 23, 1387–1395

which the organic amines are grafted to the surface of nanoporous inorganic materials. The latter combines the favorable properties of liquid−amine absorption and gas−solid adsorption, since a considerable fraction of the pore volume is available to the gases, and presents faster kinetics.[14] Also, the amine species are covalently bonded to the nanoporous material, affording the resultant inorganic−organic hybrid materials high thermal stability.[15,16]

Although a growing number of studies are available in the literature on the modification of nanoporous materials with amines for CO_2 adsorption,[5,14−32] most work is centered on the synthesis conditions, stability, regeneration, and adsorption capacity. These studies usually assume the same reaction mechanism identified for the liquid amine process. However, the nature of the molecular interaction between CO_2 gas and the grafted amine groups[5,16,22,27,29−32] remains poorly studied and is largely a matter of speculation. The few attempts to study this process have used infrared spectroscopy, which suggests the formation of carbamate, carbonate, and bicarbonate species. However, due to the low intensity, large width, and strong overlap of the infrared bands, their unambiguous assignment and quantification has not been possible. In a recent review, the divergence of results obtained by infrared techniques, regarding the nature of the species formed, was well documented, including disagreements in the assignment of the infrared bands.[33]

The present work aims at understanding at the molecular level the nature of the interaction of CO_2 with the amine-modified surface of a nanoporous material. The nanoporous materials that were studied, synthesized from natural clays (porous clays heterostructures, PCH), and modified with 3-aminopropyltriethoxysilane excel in the separation of CO_2 from several gas mixtures.[34] Besides the adsorption and characterization techniques usually employed, modified PCH samples with adsorbed carbon dioxide enriched in ^{13}C ($^{13}CO_2$) have been studied by magic-angle spinning (MAS) NMR spectroscopy. This technique allowed the comprehensive study of the interaction of CO_2 molecules with the grafted amine groups and the correlation of this information with the CO_2 adsorbed amounts, adsorption heats, and amine loadings.

EXPERIMENTAL SECTION

Material Synthesis. PCHs were prepared according to the literature.[35−39] A 5.3 cm^3 decylamine (Aldrich, 95%) solution with 35.5 cm^3 tetraethoxysilane (TEOS, Aldrich, 98%) was prepared. To this solution, 1 g of clay (a Portuguese clay, from soil deposits in Porto Santo in Madeira archipelago) was added under stirring. After mixing for 5 h, the solid was centrifuged and reacted with 10 cm^3 of deionized water while stirring for 30 min. The solid obtained was centrifuged, washed with ethanol (Panreac, 99.5%), centrifuged again, air-dried, and calcined at 650 °C for 5 h with a 1 °C min^{-1} ramp.

For the preparation of the PCH functionalized with 3-aminopropyltriethoxysilane (APTES), 2 g of PCH was mixed with 1.18 cm^3, APTES (Aldrich, 99%), and 100 cm^3 of toluene (Aldrich, >99.5%) in a reflux apparatus. The mixture was heated and kept under reflux for 24 h in nitrogen atmosphere. The resulting solid was air-dried, powdered in a mortar, and dried in an oven at 120 °C. The sample obtained was labeled PCH+APTES.

Low-Temperature Nitrogen Adsorption. Low-temperature nitrogen (Air Liquid, 99.999%) adsorption isotherms were measured in an automatic volumetric apparatus (Quantachrome, Nova 2200e), at −196 °C using a liquid nitrogen cryogenic bath. The samples, between 50 and 100 mg, were outgassed for 2.5 h at a pressure lower than 0.1 Pa. The outgassing temperature was 300 °C, for the PCH, and 150 °C, for the PCH+APTES. A lower temperature was used for the latter, to avoid decomposition of the organic groups.

Themogravimetry with Differential Scanning Calorimetry (TG-DSC). TG-DSC experiments were performed in an apparatus (Setaram, TG-DSC 111) between 30 and 300 °C. The experiments had a precision of 0.001 mg and 0.05 mW. Samples of about 40 mg in aluminum crucibles were used, with a heating rate of 1 °C min^{-1}, in nitrogen (Air Liquid, 99.995%) with a flux of 0.5 cm^3 s^{-1} measured with a glass fluxmeter (Brooks Instruments N.V., tube size R-2-15-AA).

Nitrogen Content Analysis. The nitrogen content of the PCH+APTES sample was determined by elemental analysis in an external laboratory. Briefly, the sample was burned at about 1000 °C in an oxidizing atmosphere, and the released gases were analyzed by gas chromatography with a thermal conductivity detector.

Carbon Dioxide Adsorption. The adsorption isotherms of CO_2 (Air Liquide, 99.995%) were measured in a laboratory-made stainless steel volumetric apparatus, with a 1100 kPa pressure transducer (Pfeiffer Vacuum, APR 266), equipped with a rotary/diffusion pump system, which produced a vacuum better than 10^{-2} Pa. The apparatus and adsorption cell temperatures were maintained at the experimental temperature to within 0.05 °C using a water bath (Grant, GD 120). Before experiments, samples were outgassed for 2.5 h under vacuum, using the same outgassing temperatures as in the low-temperature nitrogen adsorption experiments. The nonideality of the gas phase was taken into account using the second and third virial coefficients to calculate the adsorbed amounts.

The adsorption isotherms of carbon dioxide in PCH+APTES were also measured in a balance (C. I. Electronics, Disbal and MK2-G5) suited for vacuum and connected to a computer (C.I. Electronics, Labweigh) for recording the weight at constant time intervals. The sample (about 50 mg) was outgassed using the same conditions as in the volumetric experiments (see above). Gas doses were then introduced in the system and allowed to equilibrate with the sample. Pressure readings were made with a capacitance transducer (Pfeiffer Vacuum, CMR 262). The temperature was controlled using a water bath (Grant, GD120), with a precision of 0.05 °C.

Microcalorimetry. Heats of adsorption were measured in a Tian-Calvet type microcalorimeter (C-80, Setaram, France). In these experiments, the amounts adsorbed were determined in a volumetric apparatus, coupled to the microcalorimeter, equipped with a pressure transducer for the 0−133 kPa range (Baratron 310, MKS, USA), described in detail elsewhere.[40] Before experiments, the PCH+APTES sample of about 50 mg was outgassed for 2.5 h at 150 °C in a vacuum better than 10^{-3} Pa. Reproducibility in the determination of the amounts adsorbed was better than 0.2 μmol, and the resolution of the calorimeter was 0.1 mW. Small doses of CO_2 were successively added at increasing pressures, simultaneously measuring the amount adsorbed and the heat evolved. After correction for the so-called heat of compression, the isosteric heats of adsorption, q^{st}, were calculated. The values of q^{st} obtained from calorimetric experiments can be directly compared with those obtained from a family of adsorption isotherms at different temperatures.[41] In this way, the volumetric isotherm, n^{ads} versus p, and the differential calorimetric isotherm, q^{st} versus n^{ads}, were obtained.

Diffuse Reflectance Infrared Fourier Transform Spectroscopy. The diffuse reflectance infrared Fourier transform (DRIFT) spectra were collected on a Nicolet 6700 FTIR spectrometer at 4 cm^{-1} resolution using the smart diffuse reflectance accessory, at room temperature with a DTGS TEC detector. Before experiments, the samples were outgassed for 2.5 h at a pressure lower than 0.133 Pa and heated at 150 °C, in glass tubes with vacuum stopcocks (J. Young). Before collecting the spectrum, one of the tubes was filled with CO_2 (Air Liquide, 99.995%) and the sample was left in this atmosphere for 1 day. After this, the sample was transferred to the sample holder of the diffuse reflectance accessory and the infrared absorption spectrum was recorded.

Table 1. Textural Parameters and Nitrogen Content of the Samples

	A_{BET} [a] ($m^2\ g^{-1}$)	$V_{micro+meso}$ [b] ($cm^3\ g^{-1}$)	N content (mmol g^{-1})
PCH	847 ± 16	0.348 ± 0.002	
PCH+APTES	252 ± 1	0.081 ± 0.001	1.86 ± 0.03

[a] Determined by the Brunauer−Emmett−Teller equation. [b] Micro−plus−mesopore volume estimated by the α-plot method, using as reference a nonporous hydroxylated silica.[59]

Solid-State NMR. ^{13}C high-power decoupling (HPDEC)/cross-polarization (CP) MAS and ^{15}N CPMAS NMR spectra were recorded on a Bruker AVANCE 400 (DSX) WB spectrometer (9.4 T), using a double-resonance 4 mm probe, at 100.62 and 40.54 MHz, respectively. ^{13}C HPDEC NMR spectra were measured with a 45° flip angle (3.6 μs), 100 s recycle delay; 128−256 transients were accumulated. ^{13}C and ^{15}N CPMAS spectra were recorded using a ramped-amplitude cross-polarization (RAMP-CP) shape (100% to 50% amplitude); rf field strengths between 50 and 70 kHz for Hartman−Hahn condition calibration for ^{1}H and $^{13}C/^{15}N$ channels; number of scans for ^{13}C CPMAS: 64−256; number of scans for ^{15}N CPMAS: 52 k; recycle delay of 5 s; contact time = 1.5 ms. A power level for ^{1}H decoupling of 80 kHz during $^{13}C/^{15}N$ signal acquisition was employed for HPDEC and CPMAS experiments. ^{13}C and ^{15}N chemical shifts were externally referenced to the C=O carbonyl peak (176.03 ppm) and amine peak (δ_{NH3} = −347.6 ppm) of glycine, respectively. All the reported NMR chemical shifts, along the Results and Discussion section, have an estimated maximum interval of uncertainty equivalent to half the minimum visible ppm scale interval (±0.05 ppm).

Before adsorbing $^{13}CO_2$, the samples were previously outgassed in glass tubes with vacuum stopcocks (J. Young) connected to a vacuum line and heated at 150 °C (PCH+APTES) and at 300 °C (PCH), for 2.5 h, under a vacuum better than 10^{-2} Pa. $^{13}CO_2$ (Isotec, 99 atom % ^{13}C; <3 atom % ^{18}O) was then introduced into the tubes up to 107 kPa (Pfeiffer Vacuum, CMR 262); the tubes were closed, and the samples were kept in that atmosphere for at least 2 days. To study the $^{13}CO_2$ desorption, the glass tubes were reconnected to the vacuum line and the samples were outgassed for 4 h at ambient, 50 and 100 °C temperatures. In all cases, to record the ^{13}C and ^{15}N MAS NMR spectra, the closed tubes were taken to the NMR laboratory and immediately before starting the experiments the samples were quickly transferred to zirconia rotors and closed.

Theoretical isotropic ^{13}C chemical shifts of organic groups on the surface of the pores were calculated using GAUSSIAN 03[42] considering the molecules in the gas phase, i.e., no solvent present and with the propyl chain connected to a $Si_3O_6(OH)_3$ cluster. Geometry optimizations have been computed using the nonlocal hybrid three parameters B3LYP density functional approach[43,44] with the 6-311+G(2d,p) basis set, and the NMR shielding tensors were computed with the gauge-independent atomic orbital method.[45] The isotropic chemical shift was calculated from the isotropic shielding using as reference the isotropic shielding of tetramethylsilane (TMS). The TMS isotropic shielding was calculated using the same computational procedures at the same conditions above-described.

RESULTS AND DISCUSSION

Carbon Dioxide Adsorption and Microcalorimetry. The surface areas (A_{BET}) and porous volumes ($V_{micro+meso}$) of parent PCH and PCH grafted with APTES (PCH+APTES) are collected in Table 1. The decrease in the porous volume is ca. 77%, showing that the aminopropyl chains occupy a considerable fraction of the initial PCH porosity. The characterization of the porosity of the PCH and the PCH+APTES was already extensively discussed in a previous work.[34] Briefly, the PCH material has pores ranging from supermicropores to small mesopores, presenting a pore size distribution with a maximum at 3.2 nm and a nitrogen adsorption isotherm of type I+II in the Brunauer, Deming, Deming, and Teller classification. The PCH+APTES showed a maximum in the pore size distribution at 2.4 nm with a broad distribution of pore sizes. This reveals that functionalization with APTES reduces, on average, the pore sizes of the material, as expected, but the final material is still porous. The α_s plots of the nitrogen adsorption isotherms, used to estimate $V_{micro+meso}$, also confirmed that the PCH and PCH+APTES materials are essentially mesoporous materials with a small amount of microporous volume.[34] Considering the PCH+APTES nitrogen content, determined by chemical analysis, (Table 1) and the initial PCH surface area, a grafting density of about 1.3 ± 0.1 molecules nm^{-2} may be estimated. This value is within the range of values obtained for regular mesoporous silicas, 0.6−2.4 molecules nm^{-2} and close to 1.0−1.2 molecules nm^{-2}, typical values obtained in MCM and SBA materials.[4,14,19,20,25,46,47] For this calculation, we assumed that the surface area is reasonably estimated by the A_{BET} parameter, because the porous volume of this material is mainly mesoporous, as detailed in a previous work.[34] The difference in the maxima of the pore size distribution of the two samples indicates that the aminopropyl chains are not arranged perpendicular to the surface but rather packed over it. In fact, the results can also point to the presence of a nonhomogeneous layer of aminopropyl on the surface of the material, since the grafting density and layer thickness have relatively low values to be compatible with the presence of a homogeneous and dense layer. Nevertheless, as discussed above, the porosity characterization of PCH+APTES indicated that the material is mesoporous, although a narrowing in the pores and a lowering in the porous volume is observed, which means that a significant part of the aminopropyl chains are inside the pores. Previously reported NMR characterization of this sample has shown that APTES binds to the solid surface in bi- and tridentate modes.[34]

The CO_2 adsorption capacity of PCH+APTES is determined from the adsorption isotherms measured at different temperatures up to 1000 kPa (Figure 1). The lines represent the fitting of a virial equation, used to interpolate the experimental data (Supporting Information, Table S1). The amount of CO_2 adsorbed, especially at high pressures, decreases with increasing temperature. Up to 100 kPa (atmospheric pressure), the slope of the three curves is relatively high and the adsorbed amount does not depend much on the temperature, between 0.9 and 1.1 mmol g^{-1} at that pressure. This suggests that a strong interaction between CO_2 and the surface occurs at low pressures. Plotting the amounts adsorbed as CO_2 adsorbed amount per nitrogen content shows that the isotherms at the three temperatures are rather similar up to about 0.4 carbon dioxide molecules per nitrogen atom on the adsorbent; above this amount, the three curves begin to diverge.

To study the interaction between CO_2 and the amines on the surface of the material, it is important to evaluate the reversibility of the CO_2 adsorption and the thermal stability of the adsorbed species. In addition, for a possible application of these materials,

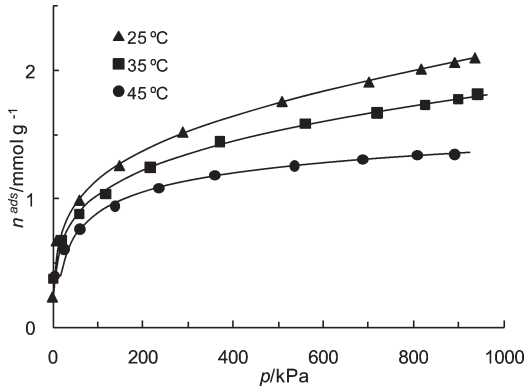

Figure 1. High-pressure adsorption isotherms of CO_2, at 25, 35, and 45 °C, on PCH+APTES (lines: virial equation fitting to experimental points; see Supporting Information).

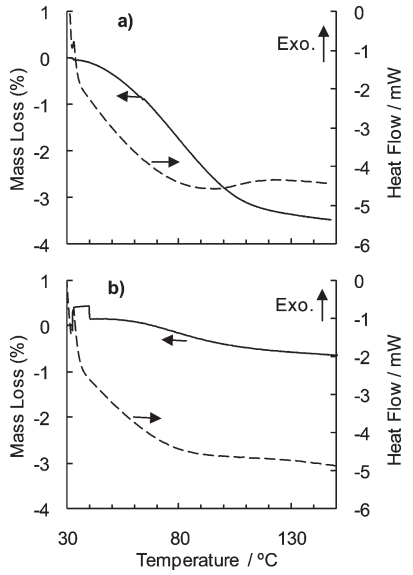

Figure 2. TG-DSC curves of PCH+APTES: (a) with and (b) without CO_2.

the regeneration of the adsorbent by temperature treatment is also of importance. The PCH+APTES regeneration capabilities and the heat involved in this process for a sample loaded with CO_2 was studied by TG-DSC (Figure 2a). The results may be compared to the results for a sample without adsorbed CO_2 (Figure 2b). The mass loss at 150 °C of the sample containing carbon dioxide was 3.43 ± 0.01%. Since the materials were previously kept in nitrogen flow for 10 min to stabilize the weight before starting the TG-DSC measurements, this value essentially corresponds to CO_2 that is bonded to the amine surface groups, rather than physically adsorbed. Figure 2a also shows that the majority of carbon dioxide is released between 60 and 100 °C, indicating that the chemical species formed by interaction of CO_2 with the amines are not very stable. The heat flow curve confirms that the process is endothermic. The integration of this curve between 35 and 150 °C and the corresponding mass loss yield a mean carbon dioxide desorption heat of 118 kJ mol^{-1}, similar to the values reported by Knöfel et al. for a ethylenediaminepropyl functionalized SBA-16[21] but larger than those measured by DTA for aminopropyl and diethylenetriaminepropyl functionalized hexagonal mesoporous silicas[20,25] and for ethylenediamine functionalized SBA-16.[18] The TG-DSC results also revealed that the organic part of the hybrid material (PCH+APTES) begins to decompose at ca. 180 °C (Supporting Information, Figure S1), as other similar amine-containing porous materials do.[25,26,47]

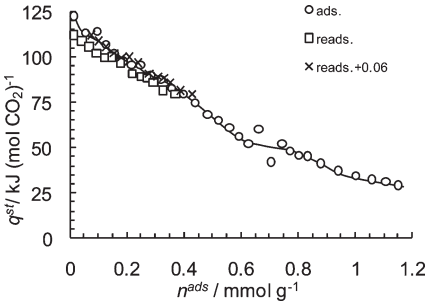

Figure 3. Differential calorimetric isotherms of CO_2 adsorption on PCH+APTES. The data corresponds to adsorption, readsorption after outgassing by vacuum for one night, and with readsorption points displaced 0.06 mmol g^{-1} to the right-hand side along the x-axis.

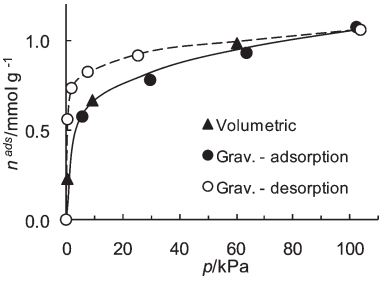

Figure 4. Adsorption and desorption isotherms of CO_2 at 25 °C, on PCH+APTES, below atmospheric pressure determined by volumetric and gravimetric methods. The lines are a guide to the eye.

The differential adsorption heat of CO_2 on the PCH+APTES sample at 37 °C, obtained by adsorption microcalorimetry, is depicted in Figure 3. Two zones can be defined. The first one is from 0 to 0.8 mmol g^{-1} where a change in the slope of the differential heat curve is envisaged. These results show a pronounced heterogeneity in the interaction between CO_2 and the surface because the heats range from 125.0 ± 0.5 kJ mol^{-1} (initial heat) to about 49 kJ mol^{-1} (at 0.8 mmol g^{-1}). A second zone is from this point onward (to higher adsorbed amounts) where the heats slowly decrease down to 29.0 ± 0.5 kJ mol^{-1} in the last measured point (near atmospheric pressure), which is close to the adsorption heat on silicalite[48] and indicates that, at this point, weak adsorption is mainly taking place on the silica pores walls. This heterogeneity on the differential heat curve, with distinct slopes, was previously reported by other authors on similar amine-modified porous materials.[21,49]

At the end of the adsorption microcalorimetric experiment, the sample was outgassed under vacuum for one night, at the experiment temperature (37 °C), and a CO_2 readsorption experiment was carried out. The readsorption isotherm points are different from the original isotherm. However, a shift of the data along the x-axis by about 0.06 mmol g^{-1} gave coincidence between the two sets of data (Figure 3). This shows that almost all CO_2 was removed by vacuum during the overnight outgassing, and most of the adsorption sites are free, even those with high-energy, ready to react with CO_2.

The reversibility was studied in more detail at low pressures by gravimetry. The results confirm that the system was close to

dx.doi.org/10.1021/cm1029563 |*Chem. Mater.* 2011, 23, 1387–1395

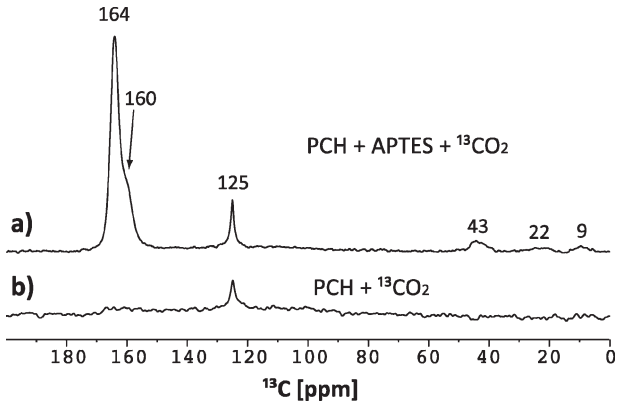

Figure 5. ^{13}C HPDEC NMR spectra of (a) PCH+APTES and (b) PCH, with adsorbed $^{13}CO_2$.

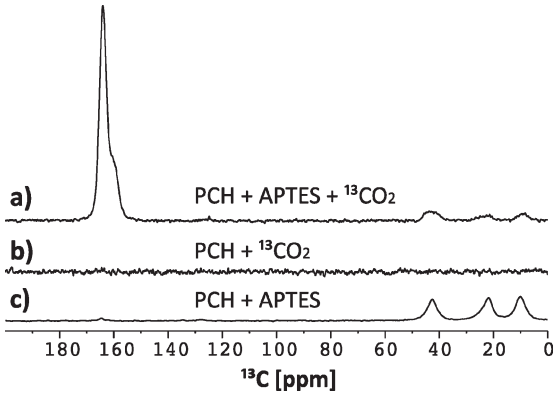

Figure 6. ^{13}C CPMAS NMR spectra of (a) PCH+APTES with $^{13}CO_2$; (b) PCH with $^{13}CO_2$; (c) PCH+APTES without $^{13}CO_2$.

equilibrium and show that it is reversible with pressure, i.e., all CO_2 can be removed by lowering the pressure (Figure 4), with some hysteresis at low pressures. The desorption kinetics was very slow, with each point taking more than 2 h to reach equilibrium, and the last point took more than 2 days. Conversely, the adsorption kinetics was rather fast. The low-pressure hysteresis and the slow-desorption kinetics are important features of the CO_2 adsorption on PCH+APTES behavior, that could not be observed with the experiments reported above.

The comparison of the DRIFT spectra of the PCH and PCH+APTES samples confirmed the presence of additional bands on the latter in the range from 2956 to 2860 cm^{-1}, attributed to the C−H stretching modes, and in the range from 1580 to 1400 cm^{-1}, assigned to the aliphatic C−H bending of the aminopropyl group, already identified in a previous work.[34] The DRIFT spectra of the PCH+APTES samples, with and without adsorbed CO_2 (Figure S2, Supporting Information), are very similar, and no new bands appear in the spectrum of the former. A small increase in the area and broadening of the band at 1600−1520 cm^{-1} is noted, but this information does not allow one to indentify the species formed on the surface. This lack of difference of the spectra indicates the limitations associated with the infrared techniques for the identification of the species formed by CO_2 on the surface of the sample with ATPES.

$^{13}CO_2$ Adsorption and NMR Studies. To understand the nature of the adsorbed CO_2 species better, samples loaded with both CO_2 and $^{13}CO_2$ at 100 kPa were studied by ^{13}C solid-state NMR spectroscopy. The ^{13}C HPDEC NMR spectrum of PCH (Figure 5 b) displays a single peak at ca. 125 ppm, attributed to CO_2 physically adsorbed. The presence of a single resonance indicates that CO_2 is the only species physically adsorbed on this sample, what is expected since no amine groups are present in PCH. However, for the PCH+APTES sample (Figure 5a), four other resonances are observed (i) three weak peaks at ca. 43, 22, and 9 ppm assigned to APTES propyl chain carbons;[34] (ii) one strong resonance at ca. 164 ppm, ascribed to carbamate species formed by reaction of CO_2 with the amine groups on the surface of the solid, already identified by other authors in the liquid phase and polymers.[50−55] In this work, we present a detailed analysis of the resonance ascribed to carbamate species in amine-functionalized materials never presented before, using $^{13}CO_2$ adsorption. The ^{13}C HPDEC NMR spectrum, obtained at a lower rotation frequency (2.5 kHz), exhibits a manifold of rotational spinning sidebands due to chemical shift anisotropy of the ca. 164 ppm ^{13}C resonance (Supporting Information, Figure S3). This is consistent with the idea that CO_2 resides inside the pores and is chemically bonded to APTES via the amine groups, forming carbamate species.

Close inspection of the peak at ca. 164 ppm reveals a shoulder, indicating that the reaction of CO_2 with the amine forms two different species (Supporting Information, Figure S4). Spectral deconvolution yields peaks at 164 ± 0.03 (73 ± 6%) and 160 ± 0.1 ppm (27 ± 2%). Values inside parentheses refer to relative peak areas in percentage. The assignment of the 160 ppm shoulder will be discussed later.

The ^{13}C CPMAS spectra of PCH+APTES and PCH after $^{13}CO_2$ saturation (Figure 6a,b) do not display the peak at ca. 125 ppm (Figure 5), confirming that this resonance is given by CO_2 molecules with high mobility. The spectrum of PCH+APTES without CO_2 (Figure 6c) only exhibits the aminopropyl chain peaks (43, 22, and 9 ppm), confirming that the 164 ppm peak is associated with the presence of CO_2 on the sample with APTES.

The reaction yielding carbamate species is expected to occur at low pressures, since it involves a strong chemical interaction with the surface of the material. Thus, this process corresponds to the low-pressure part shown in Figure 1 and discussed above and is related to the presence of amine groups on the surface of the material.

The total area of the two peaks [164 ppm (carbamate) and 125 ppm (CO_2)] due to CO_2 adsorption on PCH+APTES (Figure 5a) represents the total amount of CO_2 adsorbed. The relative areas of the peaks are ca. 93 ± 3% (164 ppm) and 7 ± 0.5% (125 ppm), providing an estimate of the concentration of carbamate species and CO_2, respectively. From the 25 °C adsorption isotherm, the total amount of adsorbed CO_2 is 1.147 ± 0.005 mmol g^{-1}, considering a pressure of 100 kPa (Figure 1). This value may be separated into two components, considering the relative areas of the NMR peaks yielding for the carbamate species a concentration of 1.06 ± 0.04 and 0.08 ± 0.01 mmol g^{-1} for the physically adsorbed CO_2. These values clearly show that, at ambient temperature and atmospheric pressure, most adsorbed CO_2 is indeed bonded to the amine groups, in agreement with the adsorption microcalorimentry results. Previous results suggest that each CO_2 molecule reacts with two amine surface groups.[5,16,22,27,29] Thus, the maximum carbamate concentration expected from the nitrogen content of the sample (Table 1) is 0.93 ± 0.01 mmol g^{-1}. The value estimated from the adsorption amount and NMR peak integration (1.06 ± 0.04 mmol g^{-1}), although higher, is close to what is expected on the basis of the nitrogen content of the sample and indicates that the CO_2 has accessibility to the amines. Other

dx.doi.org/10.1021/cm1029563 |*Chem. Mater.* 2011, 23, 1387–1395

results in the literature for analogous materials present situations that range from full accessibility to CO_2/N ratios much lower than 0.5 due to pore blockage by the organic molecules.[14,17,33,56]

Figure 7 presents the ^{15}N CPMAS NMR spectra of the PCH+APTES sample with and without adsorbed CO_2. Although the ^{15}N spectra were recorded in natural abundance (0.36% in ^{15}N), some differences between the samples may be noticed. The sample without CO_2 presents one ^{15}N resonance peak at ca. −350 ppm assigned to the amine group of the aminopropyl chain attached to the surface of the material. However, the sample with adsorbed CO_2 gives two peaks at ca. −297 and −350 ppm, assigned to the carbamate species and to the amine, respectively. These results further confirm that the adsorption of CO_2 also changes the chemical environment of the nitrogen nuclei of the amine, as expected due to interactions between the CO_2 and the NH_2-R groups.

To understand the stability of the compounds formed by CO_2 adsorption on PCH+APTES, desorption of $^{13}CO_2$ under various conditions was studied (Figure 8). Upon evacuation for 4 h, the 125 ppm peak, assigned to physically adsorbed CO_2, disappears. Interestingly, the intensity of the peak at 164 ppm, attributed to the bonded CO_2, decreases significantly and the shoulder at 160 ppm is absent. With increasing desorption temperature (50 and 100 °C), the peak at 164 ppm decreases significantly, although it is still present at 100 °C, indicating that a significant amount of CO_2 bonded to the amines remains after desorption. Considering the area of the initial peak (before desorption) and the concentration estimated above (1.06 mmol g^{-1}), the concentration of bonded CO_2 may be estimated from the relative peak areas of the ^{13}C HPDEC spectra. The results (Table 2) provide a quantitative description of CO_2 release under different conditions. The most significant factor seems to be the vacuum, since it removes ca. 85% of the bonded CO_2. This is in agreement with the results obtained by adsorption and desorption of CO_2 at low pressures (Figure 4) and microcalorimetry (Figure 3) previously discussed. When temperature is also applied, only a small desorption increase is observed (about 90% at 50 °C and 91% at 100 °C). Since desorption occurs readily at ambient temperature, the compounds formed between CO_2 and the amine are poorly stable under vacuum.

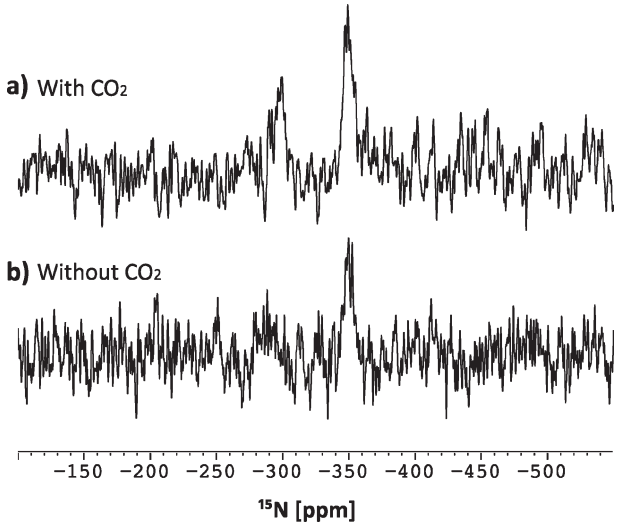

Figure 7. ^{15}N CPMAS NMR spectra of PCH+APTES (a) with and (b) without adsorbed CO_2.

The ^{13}C NMR desorption spectra (Figure 8) also assist in the assignment of the chemical species resonating at ca. 160 and 164 ppm, by depicting the stability behavior of the compounds formed when submitted to vacuum and temperature. The disappearance of the 160 ppm shoulder with vacuum and without heating, observed in both the ^{13}C HPDEC and CPMAS spectra (Figure 8), rules out the possibility of its assignment to carbonate-type species, since these only decompose at higher temperatures.[16] Moreover, some authors proposed that, in this type of material, carbonate only forms in the presence of water.[5,16,29] The possibility of assignment to urea is also ruled out because, although they have resonances at ca. 165 ppm, urea groups are only formed at high temperature in CO_2 atmosphere and are very stable with temperature,[55] contrary to what is observed in this case where the peaks intensity decrease at ambient temperature with vacuum (Figure 8). It is clear from Figure 8 that the compound producing the ca. 160 ppm peak is less stable than the carbamate (164 ppm), most likely carbamic

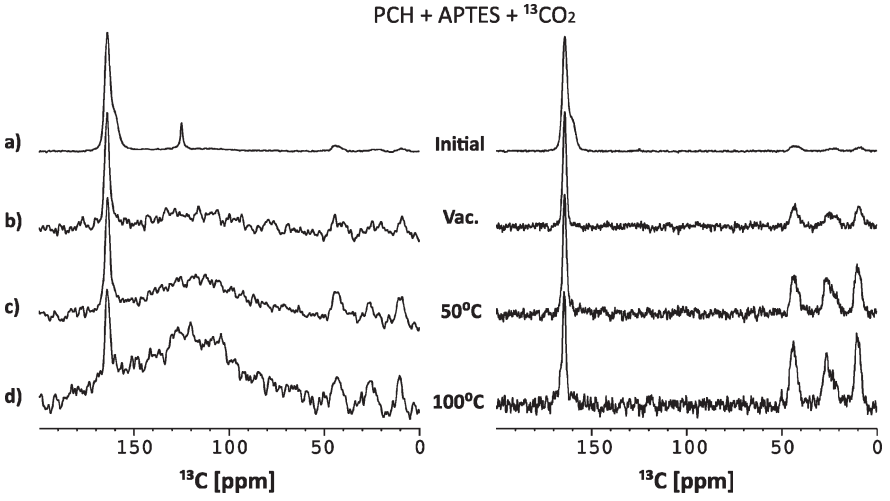

Figure 8. ^{13}C HPDEC (left) and ^{13}C CPMAS (right) NMR spectra of PCH+APTES with (a) adsorbed $^{13}CO_2$, (b) submitted to vacuum, and to vacuum and heating at (c) 50 and (d) 100 °C, for 4 h. Intensities normalized by the peak at 164 ppm. The broad hump observed between 100 and 140 ppm in (c,d) comes from probe background signal.

Table 2. Relative Intensity at 164 ppm of the ^{13}C HPDEC NMR Spectra of PCH+APTES, after Being Submitted to Different Treatments, and the Corresponding Estimated Concentration

sample treatment	relative areas at ca. 164 ppm[a]	concentration[b] (mmol g^{-1})
initial (atm. pressure)	30.8 ± 2.8	1.06 ± 0.04
vacuum 4 h	4.1 ± 0.5	0.14 ± 0.04
vacuum 4 h at 50 °C	3.0 ± 0.3	0.10 ± 0.02
vacuum 4 h at 100 °C	2.7 ± 0.3	0.09 ± 0.02

[a] Calculated using the peak areas between 175 and 145 ppm from Figure 8 (MAS spectra) and using the 9 ppm propylamine ^{13}C resonances as reference, which is assumed constant in all samples. [b] Calculated from the total adsorbed amount at 25 °C and 100 kPa (adsorption isotherm) and by taking into account the amount adsorbed as CO_2 (125 ppm) and carbamate (164 ppm). See text for further details.

acid which resonates at ca. 160 ppm.[57] It must be stressed that the interpretation of Figure 8 is not based only on the peaks chemical shift, which could be misleading, but mainly on the stability of the species with vacuum and temperature treatments. It is also worth mentioning that the presence of a shoulder at ca. 160 ppm is not related to the typical asymmetrical splitting coming from the $^{13}C-^{14}N$ dipolar-quadrupole coupling, generally observed at lower static magnetic fields (4.7 T) than the one used in this work (9.4 T).[58] However, to rule out any doubt in this regard, we have recorded a ^{13}C CPMAS spectrum at 18.8 T (Figure S5, Supporting Information), because such interaction scales inversely with the magnetic field strength (i.e., the higher the magnetic field, the weaker will be the $^{13}C-^{14}N$ interaction), and therefore, the splitting would tend to disappear as we go through stronger fields. In our case, it is clearly seen that these two peaks at ca. 160 and 164 ppm do not move when the two ^{13}C NMR spectra recorded at different magnetic fields are compared (Figure S5, Supporting Information).

The isotropic ^{13}C chemical shifts of propylcarbamate and propylcarbamic acid were calculated using GAUSSIAN 03[42] considering the molecules in the gas phase, i.e., no solvent present and with the propyl chain connected to a $Si_3O_6(OH)_3$ group. Although qualitative in nature, the values obtained for the isotropic chemical shifts were 159.2 and 165.7 ppm for, respectively, propylcarbamic acid and propylcarbamate and agree with the assignment of the experimental peaks made previously. An extended discussion on the assignment of these two peaks is further presented in the Supporting Information.

Carbamic acid is formed by the reaction of CO_2 with the amine group of APTES (first step of reaction 1), and it readily reacts with other neighboring amines to give the $RNHCOO^-/RNH_3^+$ ionic pair on the surface (second step of reaction 1). However, a fraction of carbamic acid could remain unreacted when a large amount of CO_2 is incorporated and only a small amount of R—NH_2 is still available. In this case, CO_2 produces carbamic acid, according to the first step of reaction 1, but the formed species cannot react further due to absence of neighboring amine groups. The other possibility is the existence of lone amine groups that are not sufficiently near a neighboring amine group. This may happen because of a low density of the grafting or because of a nonuniformity of amine groups on the surface. In this case, these lone groups will always form carbamic acid and not carbamate, regardless of the CO_2 pressure used.

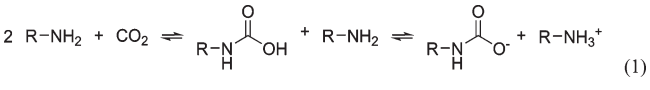

(1)

Considering the 1.06 mmol g^{-1} value of CO_2 bonded to the surface (Table 2) and the ratio of the 164 and 160 ppm peaks obtained by deconvolution of the HPDEC NMR spectra, it is possible to calculate the carbamate and carbamic acid surface amounts, respectively, 0.77 ± 0.09 and 0.29 ± 0.03 mmol g^{-1}. These values may be better compared with the nitrogen content of the sample, taking into account that the formation of each carbamate consumes two amines (2 × 0.77 mmol g^{-1}) but the formation of carbamic acid consumes only one amine (0.29 mmol g^{-1}). Following this, the amine content estimated by NMR and CO_2 adsorption is 1.8 ± 0.2 mmol g^{-1}, which is very close to the 1.86 ± 0.03 mmol g^{-1} value obtained from the nitrogen analysis of the sample. Thus, all the evidence obtained from the various experimental techniques indicates that the 164 and 160 ppm peaks arise from the acid/base equilibrium between carbamic acid/carbamate that occurs when the surface has been saturated with CO_2, under the experimental conditions in which the NMR experiments were carried out (CO_2 at atmospheric pressure).

With this information on the equilibrium at the molecular level, the differential calorimetric isotherm results (Figure 3) can be further analyzed. The end of the first zone (from 0 to 0.8 mmol g^{-1}) of higher values of the $q^{ads} - n^{ads}$ (curve of differential heat of adsorption of CO_2 vs amount adsorbed) can be tentatively ascribed to the formation of carbamate species with a stoichiometry of CO_2/APTES = 0.5, since it fairly agrees with the carbamate concentration determined above. After that, the arrival of additional CO_2 (n^{ads} > 0.8 mmol g^{-1}) is converted into carbamic acid species pushing the CO_2/APTES ratio from 0.5 toward 1.

The slow desorption kinetics results (Figure 4) may be interpreted as being associated with the energetic bonding between CO_2 and the amines (i.e., the carbamate/carbamic acid formation). In fact, putting the desorption kinetics into context with the NMR results, the release of a CO_2 molecule is only achieved after carbamic acid formation, via a proton transfer from the propylamonium to a carbamate (i.e., acid/base equilibrium, reaction 1). However, this equilibrium is highly displaced toward the carbamate and, thus, the CO_2 release is limited by this equilibrium.

CONCLUSIONS

The functionalization of nanoporous materials, prepared from natural clays, with 3-aminopropyltriethoxysilane considerably improves their CO_2 adsorption capacity at room temperature. The high initial slope of the adsorption isotherms and adsorption heat (125 kJ mol^{-1}) indicate a strong interaction between CO_2 molecules and the surface of the aminated materials.

The NMR study of $^{13}CO_2$ adsorption shows that the amount adsorbed up to atmospheric pressure is related to the number of amine groups present. Experimental evidence suggests the existence of equilibrium between carbamic acid and carbamate species formed by reaction of CO_2 on the surface of the porous material. These species are somewhat unstable, and most CO_2 is removed from the surface by evacuation, although with hysteresis at low pressures.

Nanoporous materials with amine surface groups hold potential use for CO_2 capture and may be regenerated by vacuum and/or heating. Under anhydrous conditions, the species formed with the amine groups are unstable and release CO_2 by decreasing the pressure and, thus, cyclic separation processes may be used.

Nanoporous materials functionalized with amines also catalyze the activation of CO_2, allowing its use as reactant in the synthesis of organic products.[3,4] The present work sheds light on the mechanism of such activation because CO_2 adsorption on the catalysts surface is the activation step that allows further reactions to occur. The instability of the carbamate and carbamic acid formed on the surface is important to explain the reactivity of these intermediates and supports the possible application of these materials in CO_2 activation. To be used as catalysts, the formation of carbamic acid in these materials should be maximized, since this is the unstable and reactive species. To achieve this maximization, the grafting of amine groups on the surface of porous materials should be sufficiently spaced to avoid further reaction of the carbamic acid with neighboring amine groups forming carbamate species.

■ ASSOCIATED CONTENT

Supporting Information. Details on the fit of the virial equation to CO_2 the high-pressure adsorption data and respective adjusted parameters; complete TG-DSC results of the PCH+APTES sample; DRIFT spectra of PCH+APTES samples; ^{13}C HPDEC NMR spectra of PCH+APTES at two different rotation frequencies; detailed view of the ca. 164 ppm resonance from the ^{13}C HPDEC NMR spectra of PCH+APTES with adsorbed $^{13}CO_2$; ^{13}C CPMAS NMR spectra of PCH+APTES obtained at two magnetic fields of 18.8 and 9.4 T, both with adsorbed $^{13}CO_2$; complete ref 42 (PDF). This material is available free of charge via the Internet at http://pubs.acs.org.

■ AUTHOR INFORMATION

Corresponding Author

*E-mail: moises.pinto@fc.ul.pt (M.L.P.), lmafra@ua.pt (L.M.).

■ ACKNOWLEDGMENT

M.L.P. acknowledges FCT for a postdoctoral grant (BPD/26559/2006). We thank POCT, FEDER, and FSE. Authors acknowledge financial support from Comunidad de Madrid, Spain (Project S0505/ESP/0299). L.M. is also grateful to FCT (PTDC/QUI-QUI/100998/2008).

■ REFERENCES

(1) Song, C. S. *Catal. Today* **2006**, *115* (1−4), 2–32.
(2) DOE/OS-OFE *Carbon Sequestration. State of the Science*; Office of Science and Office of Fossil Energy, U.S. Department of Energy: Washington, D.C., 1999.
(3) Srivastava, R.; Srinivas, D.; Ratnasamy, P. *J. Catal.* **2005**, *233* (1), 1–15.
(4) Srivastava, R.; Srinivas, D.; Ratnasamy, P. *Microporous Mesoporous Mater.* **2006**, *90* (1−3), 314–326.
(5) Leal, O.; Bolívar, C.; Ovalles, C.; García, J. J.; Espidel, Y. *Inorg. Chim. Acta* **1995**, *240* (1−2), 183–189.
(6) Son, W. J.; Choi, J. S.; Ahn, W. S. *Microporous Mesoporous Mater.* **2008**, *113* (1−3), 31–40.
(7) Xu, X. C.; Song, C. S.; Andresen, J. M.; Miller, B. G.; Scaroni, A. W. *Energy Fuels* **2002**, *16* (6), 1463–1469.
(8) Xu, X. C.; Song, C. S.; Andresen, J. M.; Miller, B. G.; Scaroni, A. W. *Microporous Mesoporous Mater.* **2003**, *62* (1−2), 29–45.
(9) Franchi, R. S.; Harlick, P. J. E.; Sayari, A. *Ind. Eng. Chem. Res.* **2005**, *44* (21), 8007–8013.
(10) Xu, X. C.; Song, C. S.; Miller, B. G.; Scaroni, A. W. *Ind. Eng. Chem. Res.* **2005**, *44* (21), 8113–8119.
(11) Liu, X. W.; Zhou, L.; Fu, X.; Sun, Y.; Su, W.; Zhou, Y. P. *Chem. Eng. Sci.* **2007**, *62* (4), 1101–1110.
(12) Wang, X. X.; Schwartz, V.; Clark, J. C.; Ma, X. L.; Overbury, S. H.; Xu, X. C.; Song, C. S. *J. Phys. Chem. C* **2009**, *113* (17), 7260–7268.
(13) Gray, M. L.; Soong, Y.; Champagne, K. J.; Pennline, H.; Baltrus, J. P.; Stevens, R. W.; Khatri, R.; Chuang, S. S. C.; Filburn, T. *Fuel Process. Technol.* **2005**, *86* (14−15), 1449–1455.
(14) Kim, S.; Ida, J.; Guliants, V. V.; Lin, J. Y. S. *J. Phys. Chem. B* **2005**, *109* (13), 6287–6293.
(15) Harlick, P. J. E.; Sayari, A. *Ind. Eng. Chem. Res.* **2006**, *45* (9), 3248–3255.
(16) Khatri, R. A.; Chuang, S. S. C.; Soong, Y.; Gray, M. *Energy Fuels* **2006**, *20* (4), 1514–1520.
(17) Harlick, P. J. E.; Sayari, A. *Ind. Eng. Chem. Res.* **2007**, *46* (2), 446–458.
(18) Wei, J. W.; Shi, J. J.; Pan, H.; Zhao, W.; Ye, Q.; Shi, Y. *Microporous Mesoporous Mater.* **2008**, *116* (1−3), 394–399.
(19) Huang, H. Y.; Yang, R. T.; Chinn, D.; Munson, C. L. *Ind. Eng. Chem. Res.* **2003**, *42* (12), 2427–2433.
(20) Knowles, G. P.; Graham, J. V.; Delaney, S. W.; Chaffee, A. L. *Fuel Process. Technol.* **2005**, *86* (14−15), 1435–1448.
(21) Knofel, C.; Descarpentries, J.; Benzaouia, A.; Zelenak, V.; Mornet, S.; Llewellyn, P. L.; Hornebecq, V. *Microporous Mesoporous Mater.* **2007**, *99* (1−2), 79–85.
(22) Hiyoshi, N.; Yogo, K.; Yashima, T. *Microporous Mesoporous Mater.* **2005**, *84* (1−3), 357–365.
(23) Yue, M. B.; Sun, L. B.; Cao, Y.; Wang, Z. J.; Wang, Y.; Yu, Q.; Zhu, J. H. *Microporous Mesoporous Mater.* **2008**, *114* (1−3), 74–81.
(24) Kim, S. N.; Son, W. J.; Choi, J. S.; Ahn, W. S. *Microporous Mesoporous Mater.* **2008**, *115* (3), 497–503.
(25) Knowles, G. P.; Delaney, S. W.; Chaffee, A. L. *Ind. Eng. Chem. Res.* **2006**, *45* (8), 2626–2633.
(26) Zelenak, V.; Badanicova, M.; Halamova, D.; Cejka, J.; Zukal, A.; Murafa, N.; Goerigk, G. *Chem. Eng. J.* **2008**, *144* (2), 336–342.
(27) Khatri, R. A.; Chuang, S. S. C.; Soong, Y.; Gray, M. *Ind. Eng. Chem. Res.* **2005**, *44* (10), 3702–3708.
(28) Zheng, F.; Tran, D. N.; Busche, B. J.; Fryxell, G. E.; Addleman, R. S.; Zemanian, T. S.; Aardahl, C. L. *Ind. Eng. Chem. Res.* **2005**, *44* (9), 3099–3105.
(29) Chang, A. C. C.; Chuang, S. S. C.; Gray, M.; Soong, Y. *Energy Fuels* **2003**, *17* (2), 468–473.
(30) Wang, X.; Schwartz, V.; Clark, J. C.; Ma, X.; Overbury, S. H.; Xu, X.; Song, C. *J. Phys. Chem. C* **2009**, *113* (17), 7260–7268.
(31) Knöfel, C.; Martin, C.; Hornebecq, V.; Llewellyn, P. L. *J. Phys. Chem. C* **2009**, *113* (52), 21726–21734.
(32) Bhagiyalakshmi, M.; Yun, L.; Anuradha, R.; Jang, H. *J. Porous Mater.* **2010**, *17* (4), 475–484.
(33) Choi, S.; Drese, J. H.; Jones, C. W. *ChemSusChem* **2009**, *2* (9), 796–854.
(34) Pinto, M. L.; Pires, J.; Rocha, J. *J. Phys. Chem. C* **2008**, *112* (37), 14394–14402.
(35) Galarneau, A.; Barodawalla, A.; Pinnavaia, T. J. *Nature* **1995**, *374* (6522), 529–531.
(36) Pichowicz, M.; Mokaya, R. *Chem. Commun.* **2001**, No. 20, 2100–2101.
(37) Nakatsuji, M.; Ishii, R.; Wang, Z. M.; Ooi, K. *J. Colloid Interface Sci.* **2004**, *272* (1), 158–166.
(38) Pires, J.; Araujo, A. C.; Carvalho, A. P.; Pinto, M. L.; Gonzalez-Calbet, J. M.; Ramirez-Castellanos, J. *Microporous Mesoporous Mater.* **2004**, *73* (3), 175–180.
(39) Polverejan, M.; Pauly, T. R.; Pinnavaia, T. J. *Chem. Mater.* **2000**, *12* (9), 2698–2704.
(40) Guil, J. M.; Masia, A. P.; Paniego, A. R.; Menayo, J. M. T. *Thermochim. Acta* **1998**, *312* (1−2), 115–124.

(41) Guil, J. M.; Masia, A. P.; Paniego, A. R.; Menayo, J. M. T. *J. Chem. Thermodyn.* **1994**, *26* (1), 5–14.
(42) Frisch, M. J., et al. *Gaussian 03*, Revision B.03 ed.; Gaussian, Inc.: Wallingford CT, 2003.
(43) Becke, A. D. *J. Chem. Phys.* **1993**, *98* (7), 5648–5652.
(44) Lee, C. T.; Yang, W. T.; Parr, R. G. *Phys. Rev. B* **1988**, *37* (2), 785–789.
(45) Wolinski, K.; Hinton, J. F.; Pulay, P. *J. Am. Chem. Soc.* **1990**, *112* (23), 8251–8260.
(46) Yoshitake, H.; Yokoi, T.; Tatsumi, T. *Chem. Mater.* **2002**, *14* (11), 4603–4610.
(47) Zelenak, V.; Halamova, D.; Gaberova, L.; Bloch, E.; Llewellyn, P. *Microporous Mesoporous Mater.* **2008**, *116* (1−3), 358–364.
(48) Dunne, J. A.; Mariwals, R.; Rao, M.; Sircar, S.; Gorte, R. J.; Myers, A. L. *Langmuir* **1996**, *12* (24), 5888–5895.
(49) Belmabkhout, Y.; Sayari, A. *Adsorption* **2009**, *15* (3), 318–328.
(50) Dibenedetto, A.; Aresta, M.; Fragale, C.; Narracci, M. *Green Chem.* **2002**, *4* (5), 439–443.
(51) Barzagli, F.; Mani, F.; Peruzzini, M. *Energy Environ. Sci.* **2009**, *2* (3), 322–330.
(52) Hook, R. J. *Ind. Eng. Chem. Res.* **1997**, *36* (5), 1779–1790.
(53) Bottinger, W.; Maiwald, M.; Hasse, H. *Fluid Phase Equilib.* **2008**, *263* (2), 131–143.
(54) Fan, G. J.; Wee, A. G. H.; Idem, R.; Tontiwachwuthikul, P. *Ind. Eng. Chem. Res.* **2009**, *48* (5), 2717–2720.
(55) Drage, T. C.; Arenillas, A.; Smith, K. M.; Snape, C. E. *Microporous Mesoporous Mater.* **2008**, *116* (1−3), 504–512.
(56) Serna-Guerrero, R.; Da'na, E.; Sayari, A. *Ind. Eng. Chem. Res.* **2008**, *47* (23), 9406–9412.
(57) Hampe, E. M.; Rudkevich, D. M. *Tetrahedron* **2003**, *59* (48), 9619–9625.
(58) Harris, R. K.; Olivieri, A. C. *Prog. Nucl. Magn. Reson. Spectrosc.* **1992**, *24* (5), 435–456.
(59) Gregg, S. J.; Sing, K. S. W. *Adsorption, Surface Area and Porosity*, 2nd ed.; Academic Press Inc.: London, 1982.